Search for $1_{11} - 1_{10}$ and $2_{11} - 2_{12}$ transitions of H_2CCO, H_2CCC and H_2CCCC in cosmic objects

S. Chandra[1], P.G. Musrif, R.M. Dharmkare and Monika Sharma

School of Physical Sciences, S.R.T.M. University, Nanded 431 606, India

Email: sch@iucaa.ernet.in

Abstract

Formaldehyde (H_2CO) is the first molecule observed in absorption against the cosmic microwave background (CMB) through its transition $1_{11} - 1_{10}$ at 4.829 GHz in several cosmic objects. The second line observed in a large number of cosmic objects is $2_{11} - 2_{20}$ transition at 21.59 GHz of cyclopropenylidene (c-C_3H_2) in absorption against the CMB. The phenomenon of anomalous absorption can take place under rather peculiar conditions developed in a molecule generating the line. In the present investigation, for H_2CCO, H_2CCC and H_2CCCC in cool cosmic objects, we have accounted for kinetic temperature of 10, 20, 30 and 40 K. For each of these three molecules, we have taken 30 rotational energy levels connected by 66 radiative transitions and solved the set of statistical equilibrium equations coupled with equations of radiative transfer through iterative method. We found that relative values of collisional rates can produce anomalous absorption of transitions $1_{11} - 1_{10}$ and $2_{11} - 2_{12}$ in these molecules. Anomalous absorption of $1_{11} - 1_{10}$ and $2_{11} - 2_{12}$ transitions may help in the identification of molecules in cool cosmic objects.

Key words. Interstellar molecules - H_2CCO, H_2CCC and H_2CCCC

1 Introduction

Transitiion $1_{11} - 1_{10}$ at 4.829 GHz of formaldehyde has been observed in anomalous absorption against CMB in several directions [1]. Since the energy level scheme and relative values of radiative transition probabilities for transitions between the levels in H_2CCO, H_2CCC and H_2CCCC are very similar to those for H_2CO (Table 1), in the present investigation we have discussed about the phenomenon of anomalous absorption of transitions $1_{11} - 1_{10}$ and $2_{11} - 2_{12}$ in these molecules. It has been found that a mechanism responsible for anomalous absorption depends on relative values of collisional rate coefficients. To get anomalous absorption in $1_{11} - 1_{10}$ transition, the rate coefficient for $1_{10} \rightarrow 2_{12}$ transition should be larger than that for $1_{11} \rightarrow 2_{11}$ transition. It is possible to get anomalous absorption in $2_{11} - 2_{12}$ transition.

2 Observations

Ketene (H_2CCO) is detected in Sgr B2, TMC-1 and L134N by Turner *et al.* [2], Matthews and Sears [3], Irvine *et al.* [4] and Ohishi *et al.* [5] through its transitions $4_{14} - 3_{13}$, $4_{04} - 3_{03}$,

[1]Visiting Associate, Inter-University Centre for Astronomy & Astrophysics, Pune 411 007, India

Table 1: Energy in cm^{-1} of rotational levels of ortho species and electric dipole moment

$J_{k_a k_c}$	H_2CCO	H_2CCC	H_2CCCC
1_{11}	9.6705	9.9723	9.6365
1_{10}	9.6831	9.9851	9.6390
2_{12}	11.0061	11.3465	10.2299
2_{11}	11.0438	11.3850	10.2374
3_{13}	13.0094	13.4079	11.1199
3_{12}	13.0849	13.4849	11.1349
4_{14}	15.6805	16.1563	12.3067
4_{13}	15.8063	16.2846	12.3316
5_{15}	19.0192	19.5917	13.7901
5_{14}	19.2081	19.7842	13.8274
6_{16}	23.0257	23.7142	15.5701
6_{15}	23.2901	23.9837	15.6225
7_{17}	27.6999	28.5236	17.6469
7_{16}	28.0523	28.8829	17.7166
8_{18}	33.O416	34.0200	20.0203
8_{17}	33.4948	34.4820	20.1100
9_{19}	39.0509	40.2032	22.6669
9_{18}	39.6174	40.7804	22.7790
$10_{1,10}$	45.7278	47.0732	25.6770
10_{19}	46.4202	47.7791	25.8103
3_{31}	85.0676	87.6697	85.8459
3_{30}	85.0676	87.6697	85.8459
4_{32}	87.7629	90.4427	87.0374
4_{31}	87.7629	90.4427	87.0374
5_{33}	91.1319	93.9090	88.5267
5_{32}	91.1319	93.9090	88.5267
6_{34}	95.1748	98.0685	90.3138
6_{33}	95.1748	98.0685	90.3138
7_{35}	99.8915	102.9211	92.3988
7_{34}	99.8915	102.9211	92.3988
μ(Debye)	1.41	4.1	4.5

$4_{13}-3_{12}$, $5_{15}-4_{14}$, $5_{05}-4_{04}$, $5_{14}-4_{13}$, $1_{01}-0_{00}$, $2_{02}-1_{01}$, $2_{12}-1_{11}$ and $2_{11}-1_{10}$. Molecular and distortional constants for this molecule are taken from Johns *et al.* [6] and are given in Table 2.

Propadienylidene (H_2CCC) is detected by Cernicharo *et al.* [7] and Kawaguchi *et al.* [8] in IRC +10216 and TMC-1 through its transitions $1_{01}-0_{00}$, $5_{15}-4_{14}$, $5_{14}-4_{13}$, $7_{16}-6_{15}$, $2_{12}-1_{11}$, $2_{02}-1_{01}$, $2_{11}-1_{10}$, $4_{14}-3_{13}$ and $4_{13}-3_{12}$. Molecular and distortional constants for this molecule are taken from Vrtilek *et al.* [9] and are given in Table 2.

Carbene (H_2CCCC) is detected by Cernicharo *et al.* [10] and Kawaguchi *et al.* [8] in IRC +10216 and TMC-1 through its transitions $9_{09}-8_{08}$, $10_{1,10}-9_{19}$, $11_{1,11}-10_{1,10}$, $11_{0,11}-10_{0,10}$, $11_{1,10}-10_{1,9}$, $12_{0,12}-11_{0,11}$, $12_{1,11}-11_{1,10}$, $15_{1,15}-14_{1,14}$, $15_{1,14}-14_{1,13}$, $16_{1,16}-15_{1,15}$, $2_{12}-1_{11}$, $2_{02}-1_{01}$, $2_{11}-1_{10}$, $4_{14}-3_{13}$, $4_{04}-3_{03}$, $4_{13}-3_{12}$, $5_{15}-4_{14}$, $5_{05}-4_{04}$ and $5_{14}-4_{13}$. Molecular and distortional constants for this molecule are taken from Killian *et al.* [11] and are given in Table 2.

Table 2: Molecular and distortional constants in MHz

Constants	H_2CCO*	H_2CCC†	H_2CCCC§
A	282081	288783	284468
B	10293.9772	10588.639	4503.309
C	9915.2396	10203.966	4428.616
D_J	3.394×10^{-3}	4.248×10^{-3}	0.5393×10^{-3}
D_{JK}	476.04×10^{-3}	516.4×10^{-3}	144.0×10^{-3}
D_K	23.535	23.535	0.0000
d_1	0.1453×10^{-3}	-0.153×10^{-3}	-0.0157×10^{-3}
H_{JK}	8.4×10^{-6}	7.6×10^{-6}	0.14×10^{-6}
H_{KJ}	-0.7103×10^{-3}	-1.28×10^{-3}	0.35×10^{-3}

* Johns *et al.* [6]
† Vrtilek *et al.* [9]
§ Killian *et al.* [11]

3 Basic formulation

The transitions of our interest, $1_{11}-1_{10}$ and $2_{11}-2_{12}$, belong to the ortho species of each molecule. In our investigation, NLTE occupation numbers of 30 energy levels for each molecule are calculated in an on-the-spot approximation by using the escape probability method [12], [13] where the external radiation field, impinging on a volume element generating lines, is the CMB only. In the present investigation, we solved a set of 30 simultaneous equations coupled with 66 equations of radiative transfer. This system of equations is non-linear and can be solved through iterative method for given values of hydrogen density n_{H_2} and $\gamma \equiv n_{\rm mol}/(dv_r/dr)$, where $n_{\rm mol}$ is density of molecule and dv_r/dr, the velocity gradient in cosmic object. Basic data required in this investigation are Einstein A-coefficients for radiative transitions and collisional rate coefficients between the levels.

4 Einstein A-coefficients

Treatment of an asymmetric top molecule is quite complicated as it has no preferential direction for quantization and the energy matrix is non-diagonal. Rotational wave functions for an asymmetric top molecule can be described by a linear combination of wave functions for a symmetric top molecule [14]

$$\Psi_{J\tau M}(\alpha,\beta,\gamma) = \sqrt{\frac{2J+1}{8\pi^2}} \sum_{K=-J}^{J} g^J_{\tau K} D^J_{MK}(\alpha,\beta,\gamma)$$

where α, β, γ are Euler angles specifying orientation of the molecule, J the rotational quantum number, $g^J_{\tau K}$ the expansion coefficients, D^J_{MK} the Wigner D-function and the pseudo quantum number τ is defined as

$$\tau = k_a - k_c$$

where k_a and k_c are projections of J on the axis of symmetry in case of prolate and oblate symmetric tops, respectively. Rotational levels in an asymmetric top molecule are specified as J_{k_a,k_c} or J_τ. All the three molecules, H_2CCO, H_2CCC and H_2CCCC being a-type asymmetric top, the rotational radiative transitions are governed by selection rules

$$\begin{aligned} J: &\quad \Delta J = 0, \pm 1 \\ k_a, k_c: &\quad \text{even, odd} \longleftrightarrow \text{even, even} \\ &\quad \text{odd, even} \longleftrightarrow \text{odd, odd.} \end{aligned}$$

In the representation where the axis of quantization is along a-axis of inertia, Einstein A-coefficient for transition $J'_{\tau'} \rightarrow J_\tau$ is given by [15], [16]

$$A(J'_{\tau'} \rightarrow J_\tau) = \frac{64\pi^4\nu^3\mu^2(2J+1)}{3hc^3(2J'+1)} \Big[\sum_{K=-J}^{J} g^J_{\tau K} g^{J'}_{\tau' K} C^{J'K}_{JK10} \Big]^2$$

where μ is the electric dipole moment of the molecule, and $\mathbf{C}^{\cdot\cdot}_{\cdot\cdot\cdot\cdot}$ the Clebsch Gordon coefficient. For each molecule, the Einstein A-coefficients for 66 radiative transitions between 30 energy levels are calculated and are given in Table 3.

5 Collisional rate coefficients

Computation of collisional rate coefficients is a cumbersome task. Since collisional rate coefficients are not available in the literature, scaled values for one direction (either from upper to lower or from lower to upper) can be used [17]. In the present investigation, rate coefficients for downward transition ($J'_{k'_a k'_c} \rightarrow J_{k_a k_c}$) at kinetic temperature T is taken as

$$C(J'_{k'_a k'_c} \rightarrow J_{k_a k_c}) = \frac{1\text{x}10^{-11}}{(2J'+1)} \sqrt{\frac{T}{30}} \qquad (1)$$

This relation for collisional rate coefficients can be interpreted as the cross section times a thermal velocity. For upward collisional rate coefficients, we accounted for the fact

Table 3: Einstein A-coefficients of the molecules in s^{-1}

Transitions	H_2CCO	H_2CCC	H_2CCCC
$1_{10} \rightarrow 1_{11}$	6.22×10^{-13}	5.57×10^{-12}	4.91×10^{-14}
$2_{12} \rightarrow 1_{11}$	4.46×10^{-7}	4.10×10^{-6}	3.98×10^{-7}
$2_{11} \rightarrow 1_{10}$	4.71×10^{-7}	4.34×10^{-6}	4.08×10^{-7}
$2_{11} \rightarrow 2_{12}$	5.60×10^{-12}	5.01×10^{-11}	4.42×10^{-13}
$3_{13} \rightarrow 2_{12}$	1.91×10^{-6}	1.76×10^{-5}	1.71×10^{-6}
$3_{12} \rightarrow 2_{11}$	2.02×10^{-6}	1.86×10^{-5}	1.75×10^{-6}
$3_{12} \rightarrow 3_{13}$	2.24×10^{-11}	2.00×10^{-10}	1.77×10^{-12}
$4_{14} \rightarrow 3_{13}$	4.95×10^{-6}	4.56×10^{-5}	4.42×10^{-6}
$4_{13} \rightarrow 3_{12}$	5.24×10^{-6}	4.82×10^{-5}	4.53×10^{-6}
$4_{13} \rightarrow 4_{14}$	6.22×10^{-11}	5.57×10^{-10}	4.91×10^{-12}
$5_{15} \rightarrow 4_{14}$	1.01×10^{-5}	9.33×10^{-5}	9.05×10^{-6}
$5_{14} \rightarrow 4_{13}$	1.07×10^{-5}	9.86×10^{-5}	9.28×10^{-6}
$5_{14} \rightarrow 5_{15}$	1.40×10^{-10}	1.25×10^{-9}	1.11×10^{-11}
$6_{16} \rightarrow 5_{15}$	1.80×10^{-5}	1.66×10^{-4}	1.61×10^{-5}
$6_{15} \rightarrow 5_{14}$	1.90×10^{-5}	1.75×10^{-4}	1.65×10^{-5}
$6_{15} \rightarrow 6_{16}$	2.74×10^{-10}	2.46×10^{-9}	2.17×10^{-11}
$7_{17} \rightarrow 6_{16}$	2.91×10^{-5}	2.68×10^{-4}	2.60×10^{-5}
$7_{16} \rightarrow 6_{15}$	3.08×10^{-5}	2.83×10^{-4}	2.67×10^{-5}
$7_{16} \rightarrow 7_{17}$	4.88×10^{-10}	4.37×10^{-9}	3.85×10^{-11}
$8_{18} \rightarrow 7_{17}$	4.40×10^{-5}	4.05×10^{-4}	3.93×10^{-5}
$8_{17} \rightarrow 7_{16}$	4.66×10^{-5}	4.29×10^{-4}	4.03×10^{-5}
$8_{17} \rightarrow 8_{18}$	8.06×10^{-10}	7.22×10^{-9}	6.37×10^{-11}
$9_{19} \rightarrow 8_{18}$	6.33×10^{-5}	5.83×10^{-4}	1.36×10^{-6}
$9_{18} \rightarrow 8_{17}$	6.69×10^{-5}	6.16×10^{-4}	1.43×10^{-6}
$9_{18} \rightarrow 9_{19}$	1.26×10^{-9}	1.13×10^{-8}	7.62×10^{-9}
$10_{1,10} \rightarrow 9_{19}$	8.75×10^{-5}	8.06×10^{-4}	1.70×10^{-5}
$10_{19} \rightarrow 9_{18}$	9.25×10^{-5}	8.52×10^{-4}	7.72×10^{-6}
$10_{19} \rightarrow 10_{1,10}$	1.88×10^{-9}	1.69×10^{-8}	8.38×10^{-9}
$3_{31} \rightarrow 2_{12}$	1.10×10^{-8}	9.98×10^{-8}	4.36×10^{-9}
$3_{31} \rightarrow 3_{12}$	8.90×10^{-9}	8.04×10^{-8}	3.68×10^{-9}
$3_{31} \rightarrow 4_{14}$	2.04×10^{-9}	1.84×10^{-8}	9.02×10^{-10}
$3_{30} \rightarrow 2_{11}$	1.10×10^{-8}	9.98×10^{-8}	4.36×10^{-9}
$3_{30} \rightarrow 3_{13}$	8.89×10^{-9}	8.03×10^{-8}	3.68×10^{-9}
$3_{30} \rightarrow 4_{13}$	2.04×10^{-9}	1.85×10^{-8}	9.02×10^{-10}
$4_{32} \rightarrow 3_{13}$	2.32×10^{-8}	2.09×10^{-7}	9.01×10^{-9}
$4_{32} \rightarrow 4_{13}$	2.24×10^{-8}	2.03×10^{-7}	9.28×10^{-9}
$4_{32} \rightarrow 5_{15}$	5.75×10^{-9}	5.19×10^{-8}	2.59×10^{-9}
$4_{32} \rightarrow 3_{31}$	2.37×10^{-6}	2.19×10^{-4}	2.09×10^{-6}
$4_{31} \rightarrow 3_{12}$	2.32×10^{-8}	2.10×10^{-7}	9.01×10^{-9}
$4_{31} \rightarrow 4_{14}$	2.24×10^{-8}	2.02×10^{-7}	9.28×10^{-9}
$4_{31} \rightarrow 5_{14}$	5.76×10^{-9}	5.21×10^{-8}	2.59×10^{-9}
$4_{31} \rightarrow 3_{30}$	2.37×10^{-6}	2.19×10^{-5}	2.09×10^{-6}
$5_{33} \rightarrow 4_{14}$	3.74×10^{-8}	3.38×10^{-7}	1.43×10^{-8}
$5_{33} \rightarrow 5_{14}$	3.99×10^{-8}	3.61×10^{-7}	1.65×10^{-8}

Continue table 3

Transitions	H_2CCO	H_2CCC	H_2CCCC
$5_{33} \rightarrow 6_{16}$	1.09×10^{-8}	9.82×10^{-8}	4.98×10^{-9}
$5_{33} \rightarrow 4_{32}$	6.94×10^{-6}	6.39×10^{-5}	6.10×10^{-6}
$5_{32} \rightarrow 4_{13}$	3.74×10^{-8}	3.38×10^{-7}	1.43×10^{-8}
$5_{32} \rightarrow 5_{15}$	3.98×10^{-8}	3.60×10^{-7}	1.65×10^{-8}
$5_{32} \rightarrow 6_{15}$	1.09×10^{-8}	9.85×10^{-8}	4.98×10^{-9}
$5_{32} \rightarrow 4_{31}$	6.94×10^{-6}	6.39×10^{-5}	6.10×10^{-6}
$6_{34} \rightarrow 5_{15}$	5.41×10^{-8}	4.89×10^{-7}	2.04×10^{-8}
$6_{34} \rightarrow 6_{15}$	6.11×10^{-8}	5.52×10^{-7}	2.53×10^{-8}
$6_{34} \rightarrow 7_{17}$	1.72×10^{-8}	1.55×10^{-7}	8.02×10^{-9}
$6_{34} \rightarrow 5_{33}$	1.43×10^{-5}	1.31×10^{-4}	1.25×10^{-5}
$6_{33} \rightarrow 5_{14}$	5.42×10^{-8}	4.90×10^{-7}	2.04×10^{-8}
$6_{33} \rightarrow 6_{16}$	6.09×10^{-8}	5.50×10^{-7}	2.52×10^{-8}
$6_{33} \rightarrow 7_{16}$	1.73×10^{-8}	1.56×10^{-7}	8.03×10^{-9}
$6_{33} \rightarrow 5_{32}$	1.43×10^{-5}	1.31×10^{-4}	1.25×10^{-5}
$7_{35} \rightarrow 6_{16}$	7.36×10^{-8}	6.65×10^{-7}	2.74×10^{-8}
$7_{35} \rightarrow 7_{16}$	8.60×10^{-8}	7.77×10^{-7}	3.55×10^{-8}
$7_{35} \rightarrow 8_{18}$	2.46×10^{-8}	2.22×10^{-7}	1.17×10^{-8}
$7_{35} \rightarrow 6_{34}$	2.49×10^{-5}	2.29×10^{-4}	2.19×10^{-5}
$7_{34} \rightarrow 6_{15}$	7.39×10^{-8}	6.68×10^{-7}	2.74×10^{-8}
$7_{34} \rightarrow 7_{17}$	8.55×10^{-8}	7.73×10^{-7}	3.55×10^{-8}
$7_{34} \rightarrow 8_{17}$	2.47×10^{-8}	2.23×10^{-7}	1.17×10^{-8}
$7_{34} \rightarrow 6_{33}$	2.49×10^{-5}	2.29×10^{-4}	2.19×10^{-5}

that downward and upward collisional rate coefficients are related through the detailed equilibrium [18]

$$C(J_{k_a k_c} \rightarrow J'_{k'_a k'_c}) = C(J'_{k'_a k'_c} \rightarrow J_{k_a k_c}) \, \frac{2J'+1}{2J+1} \exp\Big(-\frac{\Delta E}{kT_K}\Big) \tag{2}$$

where ΔE is the energy difference between corresponding levels. In the absence of accurate collisional rates, our results can be treated as qualitative in nature. However, the collisional rates do not create any anomalous situation from their own.

6 Anomalous absorption

Intensity, I_ν, of a line generated in an interstellar cloud, with homogeneous excitation conditions, is

$$I_\nu - I_{\nu,bg} = (S_\nu - I_{\nu,bg})(1 - e^{-\tau_\nu}) \tag{3}$$

where S_ν is source function, $I_{\nu,bg}$ is background intensity against which the line is observed, and τ_ν is optical depth of the line. Equation (3) can also be expressed as

$$B_\nu(T_B) - B_\nu(T_{bg}) = [B_\nu(T_{ex}) - B_\nu(T_{bg})](1 - e^{-\tau_\nu})] \tag{4}$$

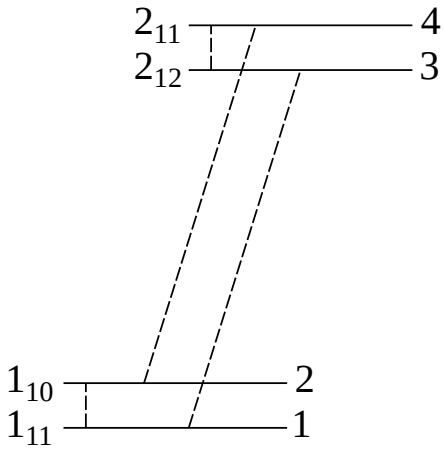

Figure 1: A set of consecutive two doublets corresponding to J = 1 and 2 levels along with the radiative transitions between them.

where B_ν represents a Planck's function corresponding to various temperatures and T_B is brightness temperature of the line. (For absorption against CMB, we have $T_B < T_{bg}$). This obviously shows that for optically thin case, $\tau_\nu \approx 0$, we have $T_B = T_{bg} \equiv 2.73$ K. Further, for Rayleigh-Jeans limit [ν(GHz) << 21 T(K)], the Equation (4) can be written as

$$T_B = T_{ex} + (T_{bg} - T_{ex})e^{-\tau_\nu} \tag{5}$$

For anomalous absorption, we have $T_{ex} < T_{bg}$ and $\tau_\nu > 0$, and therefore, $T_B > T_{ex}$. When τ_ν is very large, for anomalous absorption, we have $T_B = T_{ex}$. It shows that for anomalous absorption, brightness temperature of the line lies between T_{ex} and T_{bg} ($T_{ex} < T_B < T_{bg}$).

7 Results

In our model, free parameters are n_{H_2} and γ. In order to include large number of cosmic objects, where H_2CCO, H_2CCC and H_2CCCC may be found, numerical calculations are carried out for wide ranges of physical parameters. In the present investigation, we have taken $\gamma = 10^{-5}$ and 10^{-4} cm^{-3} (km/s)$^{-1}$ pc. The molecular hydrogen density is varied over a range from 10^2 to 10^5 cm^{-3}, and calculations are performed for kinetic temperatures of 10, 20, 30 and 40 K, as temperature in a cool cosmic object would not be more than this value.

All energy levels of these molecules are in the form of K doublets. The observed lines in absorption are due to transitions between the levels of a doublet. In order to understand the phenomenon of anomalous absorption in $1_{11} - 1_{10}$ transition, let us consider two successive doublets as shown in Figure 1.

For $1_{11} - 1_{10}$ transition, levels of $J = 1$ doublet are radiatively connected to the levels of $J = 2$ doublet only as there is no doublet in lower direction. In optically thin limit ($n_{H_2}C_{ul} << A_{ul}$), for these four energy levels, statistical equilibrium equations are

$$\begin{aligned}
n_1 n_{H_2}(C_{13} + C_{14}) &= n_3 A_{31} \\
n_2 n_{H_2}(C_{23} + C_{24}) &= n_4 A_{42} \\
n_3 A_{31} &= n_1 n_{H_2} C_{13} + n_2 n_{H_2} C_{23} \\
n_4 A_{42} &= n_1 n_{H_2} C_{14} + n_2 n_{H_2} C_{24}
\end{aligned}$$

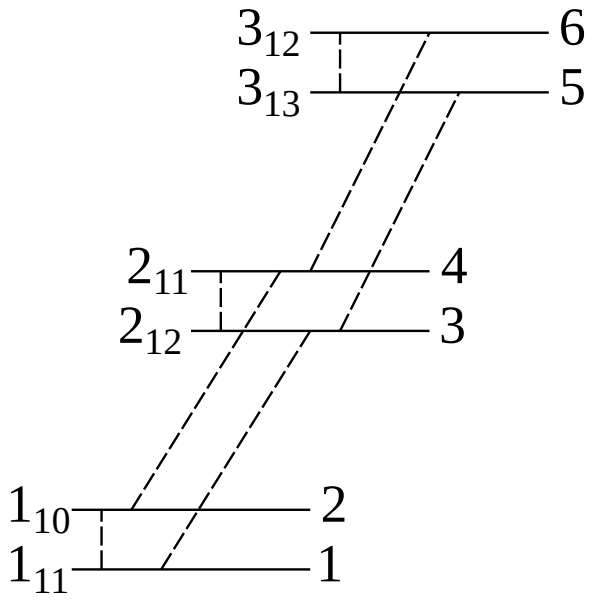

Figure 2: A set of consecutive three doublets corresponding to J =1, 2 and 3 levels along with the radiative transitions between them.

These equations can be rearranged as

$$n_2/n_1 = C_{14}/C_{23} \tag{6}$$

For absorption against the CMB, $n_2 < n_1$, showing that $C_{14} < C_{23}$. This criterion is the same as derived by Townes and Cheung [19] semiclassically and by Green *et al.* [20] quantum mechanically. Thus, when collisional rate for $1_{11} - 2_{11}$ transition is smaller than that for $1_{10} - 2_{12}$ transition, the transition between 1_{11} and 1_{10} levels would show absorption against CMB. This has been the case for explanation of $1_{11} - 1_{10}$ transition of H_2CO where collisional rates reported by Green *et al.* [20] supported this condition.

In order to understand the phenomenon of anomalous absorption in $2_{11}-2_{12}$ transition, let us consider three successive doublets as shown in Figure 2. In optically thin limit, for these six energy levels, the statistical equilibrium equations are

$$\begin{aligned}
&n_1 n_{H_2}(C_{13} + C_{14} + C_{15} + C_{16}) = n_3 A_{31} \\
&n_2 n_{H_2}(C_{23} + C_{24} + C_{25} + C_{26}) = n_4 A_{42} \\
&n_3(A_{31} + n_{H_2} C_{35} + n_{H_2} C_{36}) = n_1 n_{H_2} C_{13} + n_2 n_{H_2} C_{23} + n_5 A_{53} \\
&n_4(A_{42} + n_{H_2} C_{45} + n_{H_2} C_{46}) = n_1 n_{H_2} C_{14} + n_2 n_{H_2} C_{24} + n_6 A_{64} \\
&n_5 A_{53} = n_1 n_{H_2} C_{15} + n_2 n_{H_2} C_{25} + n_3 n_{H_2} C_{35} + n_4 n_{H_2} C_{45} \\
&n_6 A_{64} = n_1 n_{H_2} C_{16} + n_2 n_{H_2} C_{26} + n_3 n_{H_2} C_{36} + n_4 n_{H_2} C_{46}
\end{aligned}$$

This gives

$$\frac{n_4}{n_3} = \frac{n_{H_2} C_{36}}{A_{42} + n_{H_2} C_{45}} + \frac{n_1}{n_3} \frac{n_{H_2} C_{16} + n_{H_2} C_{14}}{A_{42} + n_{H_2} C_{45}} + \frac{n_2}{n_3} \frac{n_{H_2} C_{26} + n_{H_2} C_{24}}{A_{42} + n_{H_2} C_{45}} \tag{7}$$

Thus, for absorption between levels 3 and 4, we must have $n_4 < n_3$.

For $1_{11} - 1_{10}$ transition, equation (6) show that $C(1_{11} - 2_{11})$ must be smaller than $C(1_{10} - 2_{12})$. Our equation (1) gives $C(1_{11} - 2_{11}) \approx C(1_{10} - 2_{12})$, and therefore, we

reduced rate $C(1_{11} - 2_{11})$ and its reverse by a factor of 2 with respect to that of the calculations from equations (1) and (2), which is not very large. The effect of this is visible in Figure 3 (H_2CCCC), Figure 5 (H_2CCC) and Figure 7 (H_2CCO). It is interesting to note that there are remarkable changes. The results support anomalous absorption of $1_{11}-1_{10}$ transition. In this case transition $2_{11}-2_{12}$ shows very weak anomalous absorption.

For $2_{11} - 2_{12}$ transition, equation (7) says that n_4 must be smaller than n_3. In our investigation, we reduced the rates $C(3_{12} - 2_{12})$, $C(3_{12} - 1_{11})$, $C(3_{12} - 1_{10})$, $C(2_{11} - 1_{11})$, $C(2_{11} - 1_{10})$ and their reverse by a factor of 2 with respect to that of the calculations from equations (1) and (2). The results are shown in Figure 4 (H_2CCCC), Figure 6 (H_2CCC) and Figure 8. In this case, we found anomalous absorption of $1_{10} - 1_{11}$ and $2_{11} - 2_{12}$ transitions. Thus collisional rates are responsible for anomalous absorption in these molecules.

For each of these molecules, with increase of kinetic temperature, the anomalous absorption is found to decrease and position of minimum value of brightness temperature (T_B) as well as maximum value of optical depth (τ) is found to shift towards the region of low density. It shows that the possibility of identification of molecules is large in cool cosmic objects.

8 Conclusions

Under the situation that the collision rate coefficient $C(1_{11} - 2_{11})$ is smaller than $C(1_{10} - 2_{12})$, it has been found that both the transitions $1_{11} - 1_{10}$ and $2_{11} - 2_{12}$ show absorption against CMB, but absorption found in the second transition $2_{11} - 2_{12}$ is weak as compared to that of transition $1_{11} - 1_{10}$.

When collisional rate coefficients $C(3_{12} - 2_{12})$, $C(3_{12} - 1_{11})$, $C(3_{12} - 1_{10})$, $C(2_{11} - 1_{11})$, $C(2_{11} - 1_{10})$ and their reverse are reduced by a factor of 2 with respect to that of the calculations from equations (1) and (2) , anomalous absorption in both the transitions $1_{11} - 1_{10}$ and $2_{11} - 2_{12}$ is found increased. Thus, the collisional rates are responsible for the anomalous absorption. Position of the minimum value of brightness temperature (T_B) and of the maximum value of optical depth (τ) is found to shift towards the low density region with increase of kinetic temperature. Hence, the anomalous absorption decreases with increase of kinetic temperature.

In cool cosmic objects where kinetic temperature is not sufficiently high to generate emission spectrum of a molecule, detection of absorption of these transitions may help in the identification of the molecule there, as low energy levels are populated even at low temperatures.

Acknowledgments

We are grateful to Prof. Jayant V. Narlikar and Prof. Dr. W.H. Kegel for their encouragement. Thanks are due to Mr. S.V. Shinde for helpful discussion and valuable cooperation. Constructive comments from anonymous refrees are thankfully acknowledged. Financial support in the form of visits of the authors to IUCAA, Pune is thankfully acknowledged.

References

[1] P. Palmer, B. Zuckerman, D. Buhl, L.E. Snyder, *ApJ* **156** (1969) L147.

[2] B.E. Turner, *ApJ* **213** (1977) L75.

[3] H.E. Matthews, T.J. Sears, *ApJ* **300** (1986) 766.

[4] W.M. Irvine, P. Friberg, N. Kaifu, K. Kawaguchi, Y. Kitamutra, H.E. Matthews, Y. Minh, S. Saito, N. Ukita, S. Yamamoto, *ApJ* **342** (1989) 871.

[5] M. Ohishi, K. Kawaguchi, N. Kaifu, W.M. Irvine, Y. C. Minh, S. Yamamoto, S. Saito, *Atoms, ions and molecules: New results in spectral line astrophysics, ASP Conference Series (ASP: San Francisco)* **16** (1991) 387.

[6] J.W.C. Johns and J.M.R. Stone *J. mol. spectroscopy* **42** (1972) 523.

[7] J. Cernicharo, C.A. Gottlieb, M. Guelin, T.C. Killian, G. Paubert, P. Thaddeus, J.M. Vrtilek, *ApJ* **368** (1991a) L39.

[8] K. Kawaguchi, N. Kaifu, M. Ohishi, S.I. Ishikawa, Y. Hirahara, S. Yamamoto, S. Saito, S. Takano, A. Murakami, J.M. Vrtilek, C.A. Gottlieb, P. Thaddeus, W.M. Irvine, *PASJ* **43** (1991) 607.

[9] J.M. Vrtilek, C.A. Gottlieb, E.W. Gottlieb, T.C. Killian, P. Thaddeus, *ApJ* **364** (1990) L53.

[10] J. Cernicharo, C.A. Gottlieb, M. Guelin, T.C. Killian, P. Thaddeus, J.M. Vrtilek, *ApJ* **368** (1991b) L43.

[11] T.C. Killian, J.M. Vrtilek, C.A. Gottlieb,E.W. Gottlieb, P. Thaddeus, *ApJ* **365** (1990) L89.

[12] E. Rauch, W.H. Kegel, T. Tusji, G. Piehler, *A&A* **315** (1996) 533.

[13] S. Chandra, P.G. Musrif, R.M. Dharmkare, *New Astronomy* **10** (2005) 385.

[14] S. Chandra, D.A. Varshalovish, W.H. Kegel, *A&AS* **55** (1984) 51.

[15] S. Chandra, Sahu, *A&A* **272** (1993) 700.

[16] S. Chandra, Rashmi, *A&AS* **131** (1998) 137.

[17] A. K. Sharma, S. Chandra, *A&A* **376** (2001) 333.

[18] S. Chandra, W.H. Kegel, *A&AS* **142**, (2000) 113.

[19] C.H. Townes, A.C. Cheung, *ApJ* **157** (1969) L103.

[20] S. Green, B.J. Garrison, W.A. Lester Jr., W.H. Miller, *ApJ Suppl.* **37** (1978) 321.

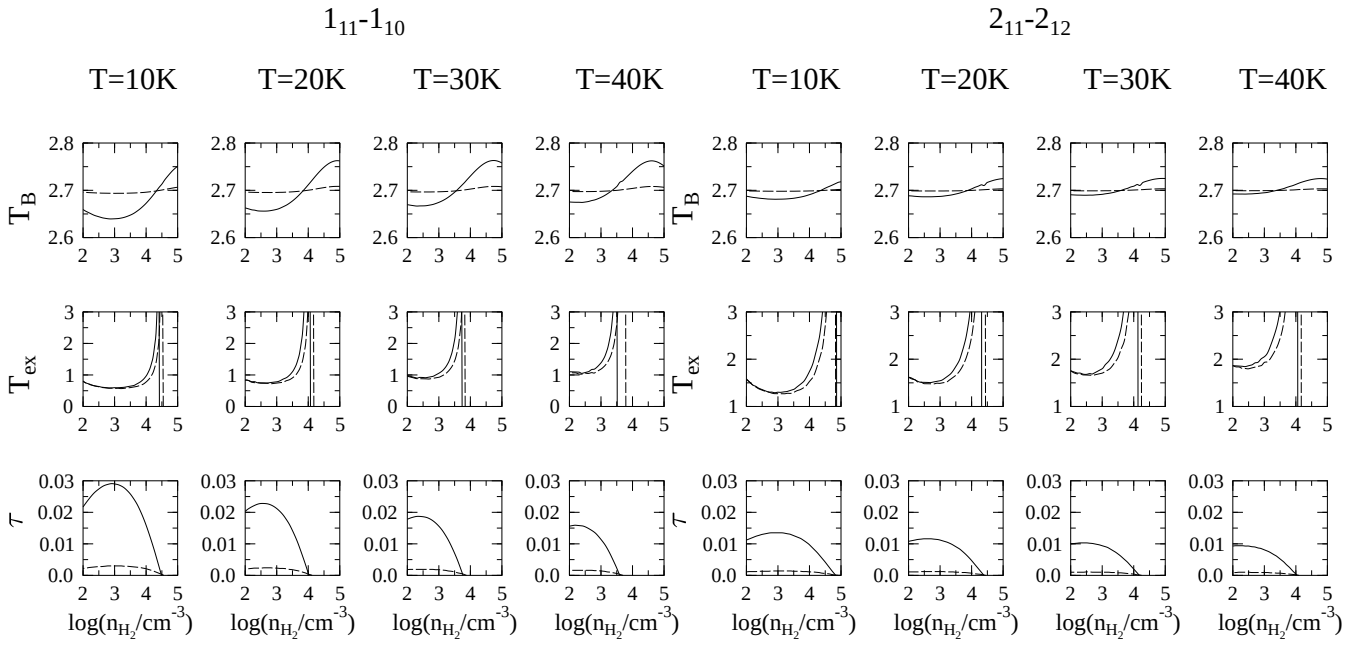

Figure 3: Variation of brightness temperature T_B (K), excitation temperature T_{ex} (K) and optical depth τ versus hydrogen density n_{H_2} of the lines $1_{11}-1_{10}$ (columns 1, 2, 3 and 4) and $2_{11}-2_{12}$ (columns 5, 6, 7 and 8) for kinetic temperature 10, 20, 30 and 40 K for H_2CCCC. Solid line is for γ =10^{-5} cm^{-3} (km/s)$^{-1}$ pc, and the dotted line for $\gamma = 10^{-4}$ cm^{-3} (km/s)$^{-1}$ pc. Collision rates of the transition $2_{11}-1_{11}$, and its reverse are reduced by a factor 2 with respect to that of the calculations from equations (1) and (2).

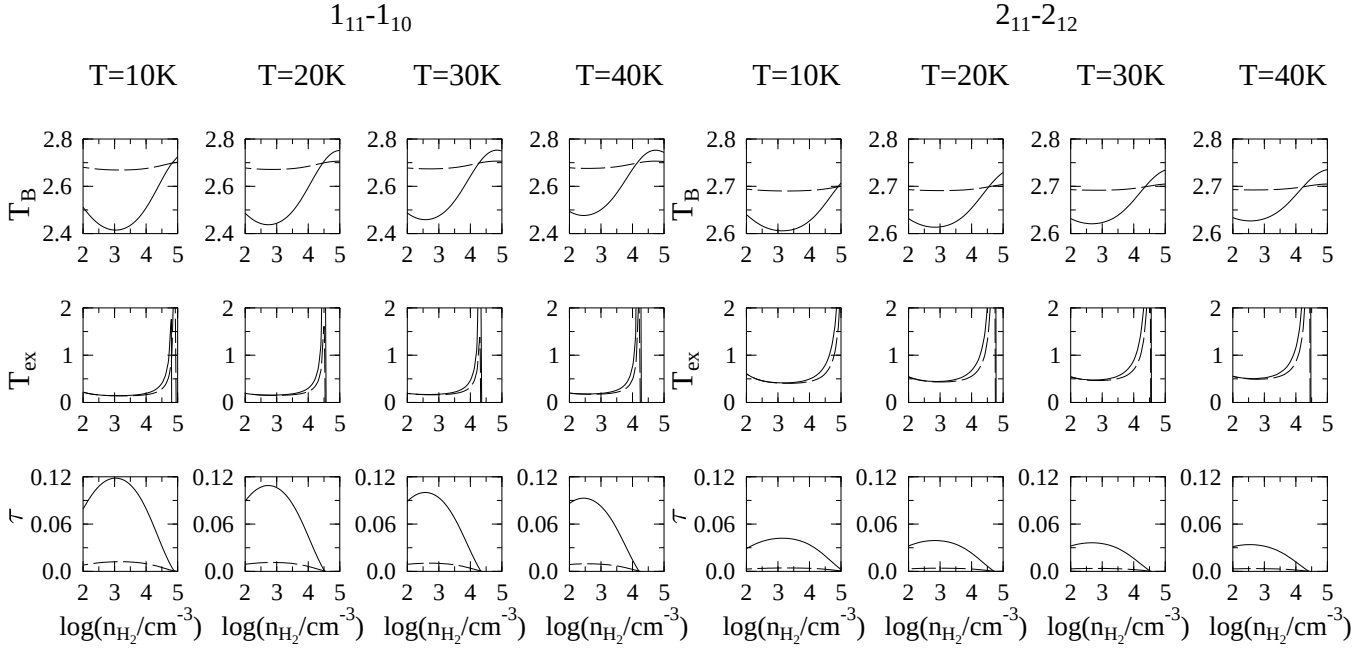

Figure 4: Same as the Figure 3, but the collisional rates of the transitions $3_{12}-1_{11}$, $3_{12}-1_{10}$, $3_{12}-2_{12}$, $2_{11}-1_{11}$ and their reverse are reduced by a factor 2 with respect to that of the calculations from equations (1) and (2).

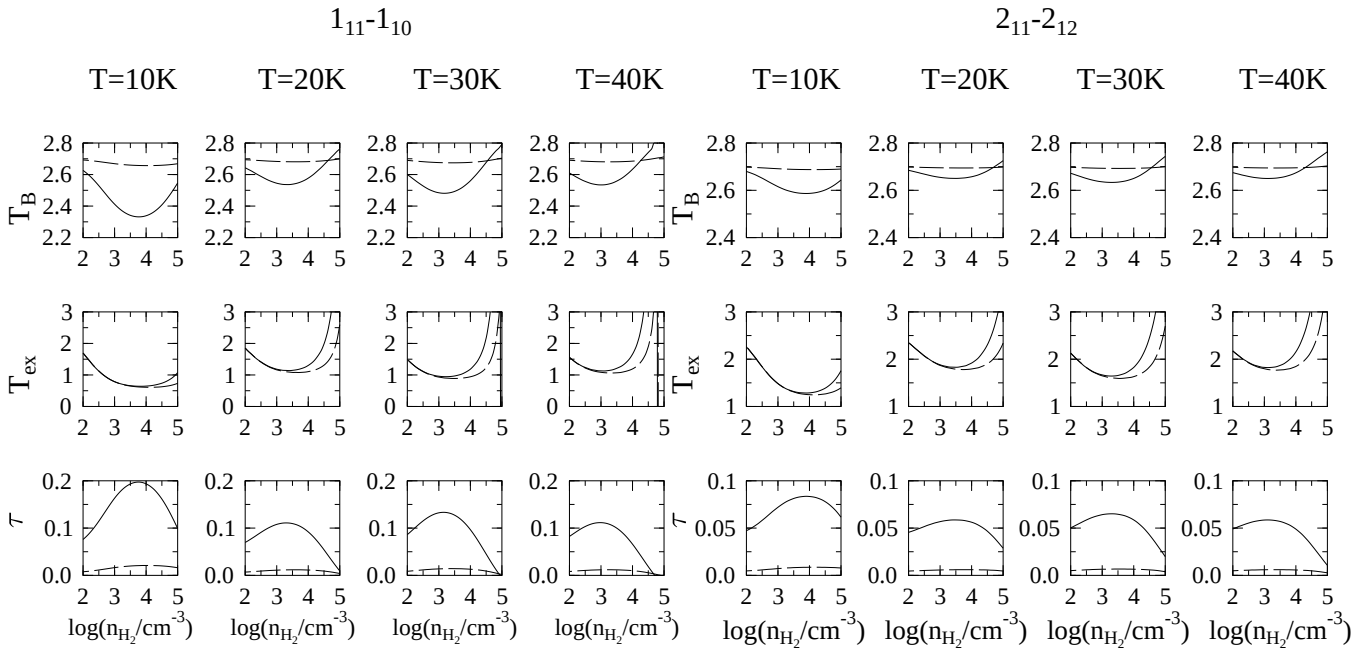

Figure 5: Variation of brightness temperature T_B (K), excitation temperature T_{ex} (K) and optical depth τ versus hydrogen density n_{H_2} of the lines $1_{11}-1_{10}$ (columns 1, 2, 3 and 4) and $2_{11}-2_{12}$ (columns 5, 6, 7 and 8) for kinetic temperature 10, 20, 30 and 40 K for H_2CCC. Solid line is for γ =10^{-5} cm^{-3} (km/s)$^{-1}$ pc, and the dotted line for $\gamma = 10^{-4}$ cm^{-3} (km/s)$^{-1}$ pc. Collision rates of the transition $2_{11}-1_{11}$, and its reverse are reduced by a factor 2 with respect to that of the calculations from equations (1) and (2).

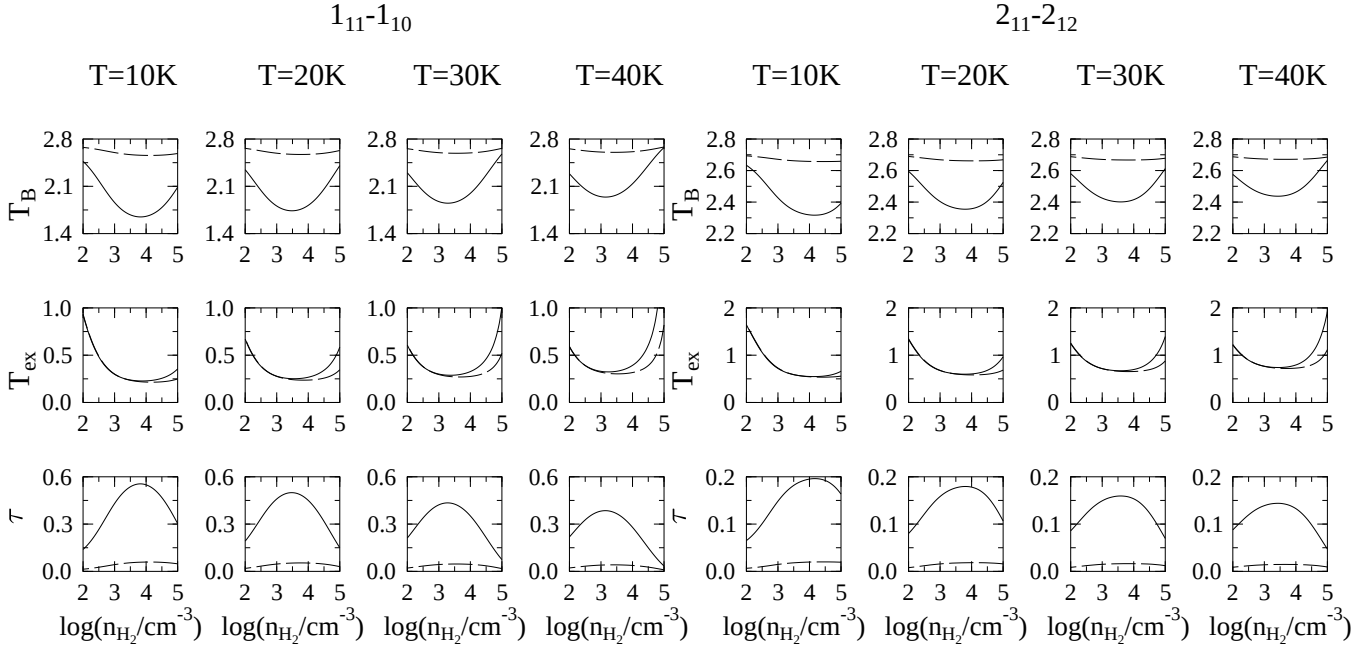

Figure 6: Same as the Figure 5, but the collisional rates of the transitions $3_{12}-1_{11}$, $3_{12}-1_{10}$, $3_{12}-2_{12}$, $2_{11}-1_{11}$ and their reverse are reduced by a factor 2 with respect to that of the calculations from equations (1) and (2).

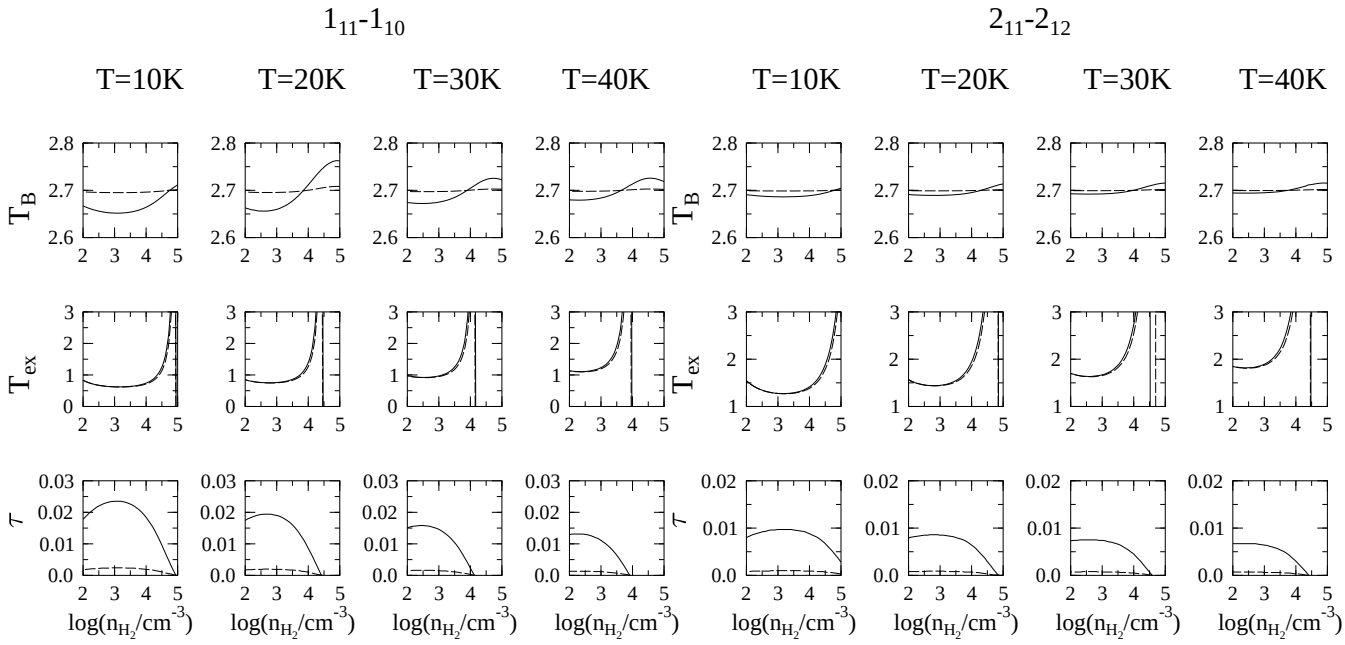

Figure 7: Variation of brightness temperature T_B (K), excitation temperature T_{ex} (K) and optical depth τ versus hydrogen density n_{H_2} of the lines $1_{11}-1_{10}$ (columns 1, 2, 3 and 4) and $2_{11}-2_{12}$ (columns 5, 6, 7 and 8) for kinetic temperature 10, 20, 30 and 40 K for H_2CCO. Solid line is for γ =10^{-5} cm^{-3} (km/s)$^{-1}$ pc, and the dotted line for $\gamma = 10^{-4}$ cm^{-3} (km/s)$^{-1}$ pc. Collision rates of the transition $2_{11}-1_{11}$, and its reverse are reduced by a factor 2 with respect to that of the calculations from equations (1) and (2).

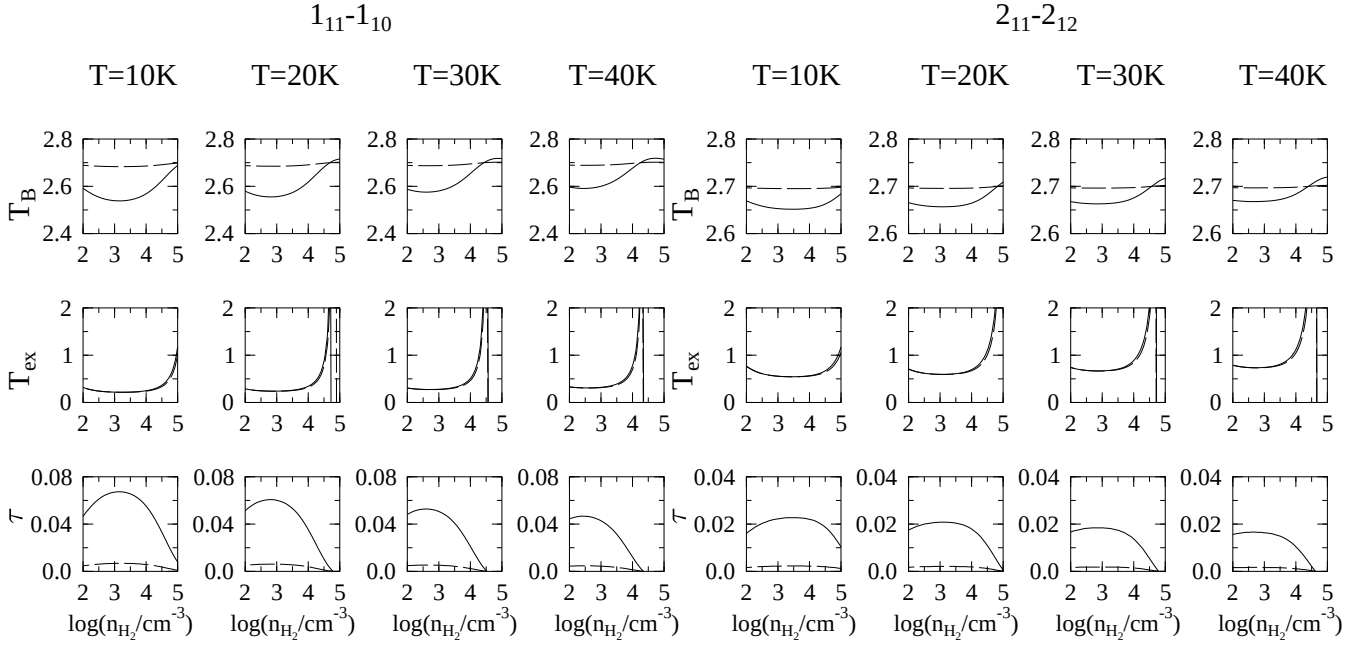

Figure 8: Same as the Figure 7, but the collisional rates of the transitions $3_{12}-1_{11}$, $3_{12}-1_{10}$, $3_{12}-2_{12}$, $2_{11}-1_{11}$ and their reverse are reduced by a factor 2 with respect to that of the calculations from equations (1) and (2).